Peer-reviewed version available at *Energies* **2017**, *10*, 911; doi:10.3390/en10070911

Article

Optimization of Guide Vane Closing Schemes of Pumped Storage Hydro Unit Using an Enhanced Multi-Objective Gravitational Search Algorithm

Jianzhong Zhou[a,b,*], Yanhe Xu[a,b,*], Yang Zheng[a,b], Yuncheng Zhang[a,b]

[a] School of Hydropower and Information Engineering, Huazhong University of Science and Technology, Wuhan 430074, China

[b] Hubei Key Laboratory of Digital Valley Science and Technology, Huazhong University of Science and Technology, Wuhan 430074, China

Abstract: The optimization of guide vane closing schemes (OGVCS) of pumped storage hydro unit (PSHU) is the research field of cooperative control and optimal operation of pumped storage, wind power and solar power generation. This paper presents a OGVCS model of PSHU considering the rise rate of the unit rotational speed and the specific node pressure of each hydraulic unit, as well as various complicated hydraulic and mechanical constraints. OGVCS model is formulated as a multi-objective optimization problem to optimize conflictive objectives, i.e., unit rotational speed and water hammer pressure criteria. In order to realize the efficient solution of the OGVCS model, an enhanced multi-objective bacterial-foraging chemotaxis gravitational search algorithm (EMOBCGSA) is proposed to solve this problem, which adopts population reconstruction, adaptive selection chemotaxis operator of local searching strategy and Elite archive set to efficiently solve the multi-objective problem. Especially, novel constraints-handling strategy with eliminating and local search based on violation ranking is used to balance various hydraulic and mechanical constraints. Finally, simulation cases of complex extreme operating conditions (i.e., load rejection and pump outage) of 'single tube-double units' type PSHU system are conducted to verify the feasibility and effectiveness of the proposed EMOBCGSA in solving OGVCS problem. The simulation results indicate that the proposed EMOBCGSA can provide lower rise rate of the unit rotational speed and smaller water hammer pressure than other method established recently while considering various complex constraints in OGVCS problem.

Keyword: pumped storage hydro unit; guide vane closing schemes; multi-objective optimization; enhanced multi-objective bacterial-foraging chemotaxis gravitational search algorithm (EMOBCGSA); hydraulic and mechanical constraints

1. Introduction

In recent years, in order to improve the global greenhouse effect and the carbon dioxide emissions, wind power, solar power generation, biomass energy and other renewable energy to maintain rapid development momentum in China[1, 2]. Grid installed capacity and power generation of new energy continued to grow, which effectively alleviate the economic development of coal, oil and other fossil energy dependence, promoting the reform of the energy structure and the development of green energy. However, due to wind and solar power are intermittent and random fluctuation characteristics, makes the grid for renewable energy consumptive ability seriously insufficient, has intensified the contradiction between the development and utilization of new energy.

* Corresponding Author: Jianzhong Zhou, Yanhe Xu. Tel.: +86 02787543127. E-mail address: jz.zhou@hust.edu.cn (J.Z.), xuyanhe2010@126.com (Y.X.).

As a special energy storage power supply, wind power-pumped storage plant (PSP) and solar power-PSP are used as the most common centralized and large-scale renewable energy complementary operation means[3-7]. The flexibility of PSP makes up for the randomness and heterogeneity of wind power and solar power generation, which is helpful to improve the reliability of the power grid and promote the integration of renewable energy variables.

The optimization of guide vane closing schemes (OGVCS) of PSHU is the research field of cooperative control and optimal operation of pumped storage, wind power and solar power generation. During the dynamic process of extreme condition (i.e. load rejection or pump outage) with the non optimal closing law, the rise of the unit rotational speed and the water hammer pressure will exceed the maximum design value, which cause the runaway speed of the PSHU, abnormal vibration or active guide vane asynchronous and other negative phenomena[8, 9]. OGVCS plays an important role in ensuring the security and stability of the power grid, and several methods have been proposed to deal with the OGVCS problem. Based on the characteristics of the rigid water-column pressure during the transient process, Ref [10] proposed a two-phase guide-vane closing scheme and three-phase valve-closing schemes to control the pulsating pressures and the runaway speed. Ref [11] analysing the effect of valve closure on the water-hammer pressure and laid the theoretical foundation for improving the turbine guide-vane closure. In order to avoid the operating point from the 'S' characteristic area, Kuwabara et al. proposed a curved closing scheme that could effectively decrease the water-hammer pressure[12]. Additionally, appropriate two-phase closing scheme[13, 14] and misaligned guide-vane method[15-17] also have been applied to control the fluctuation of PSHU. Three-phase valve-closing and curved closing scheme exerted high demands on the governor servomotor, which are difficult to realize in PSP. Meantime, misaligned guide-vane method can significantly increase the pulsating pressure and the runner radial forces during start-up process of PSHU[17]. Therefore, the optimal closing schemes are required to realize optimal coordinated operation of PSP and new energy generation technologies based on deeply analysis of operational mechanism and flow characteristics of PSHU.

Fully consider the complex hydraulic, mechanical and electrical coupling characteristics and nonlinear dynamic response process of PSHU, a multi-objective optimization model of guide vane closing schemes is established in this paper, which includes hydraulic and mechanical multiple constraint factors. The OGVCS problem is a complex, multi-objective and multi-constraint optimization problem, which aims to reasonably control the rotational speed, water hammer pressure of volute, draft tube, surge tank and so on, simultaneously. Multi-objective intelligent optimization algorithm is an effective way to solve complex multi-objective problems. Many intelligent optimization algorithms, such as PSO, GSA and so on, are widely used in solving multi-objective optimization problems multi-objective particle swarm optimization (MOPSO) [18, 19], non-dominated sorting genetic algorithm-II (NSGA-II) [20], multiobjective differential evolution (MODE) [21, 22], multi-objective gravitational search algorithm (MOGSA) [23, 24] and multi-objective bee colony optimization algorithm (MOBCO) [25, 26], have been proposed to solve the complex multi-objective optimization problems with practical modeling of coupling constraints efficiently. However, premature phenomenon and local convergence are still common obstacles to the performance of these stochastic searching algorithms. Bacterial-foraging chemotaxis gravitational search algorithm (BCGSA) is enhanced by Pbest-Gbest-guided movement, adaptive elastic-ball method and chemotaxis operator strategy of bacterial-foraging algorithm [27]. Global exploration and local exploitation performance of BCGSA have been proved by ref [27]. Inspired by the NSGA-II, EMOBCGSA has been introduced to deal with the OGVCS by reconstructing the optimal structure and mechanism. Finally, cases of complex extreme operating conditions of 'single tube-double units' type PSHU system are conducted to verify the feasibility and effectiveness of the proposed EMOBCGSA in solving OGVCS problem.

The remaining part of this paper is organized as follows. Section 2 introduces numberical calculation modeling of 'single tube-double units' type PSHU system. Section 3 establishes a multi-objective optimization model of guide vane closing schemes and multiple constraints are introduced simultaneously. Section 4 delineates the general procedure and multi-objective improvements in

BCGSA. Section 5 illustrates the practical solving procedure for OGVCS problem and experiment results along with a few discussions, respectively. The conclusions are summarized in section 6.

2. Numerical calculation model of PSHU system

'single tube-double units' type PSHU system is a kind of coupling system of hydraulic, mechanical and electrical factors, simplified mainly into four parts, namely reservoir, pressure water pipeline, surge tank and pumped storage hydro unit. Fig.1 shows the schematic diagram of 'single tube-double units' type PSHU system of this paper, we divide the system into reservoir of upstream and downstream, eight pressure water pipelines, surge tank of upstream and downstream, two PSHU. In this section, mathematical model each link is illuminated respectively.

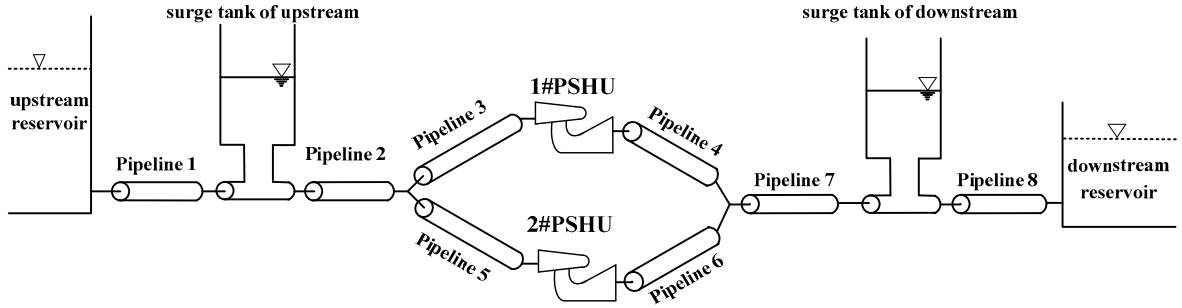

Fig.1 Structure of 'single tube-double units' type PSHU system

2.1 Model of pressure water pipeline

And, the characteristics method is employed in the modeling of pressure water pipeline, basic motion equation and continuous equation of unsteady flow in pressure pipeline can be expressed by the formulas (1) and (2) [28]. Solving the formulas (1) and (2) using the method of characteristics, which transforms formulas into a simplified equation set in the range of the characteristic line $\frac{dx}{dt}=\pm a$. The simplified equation set is described as the formulas (3) and (4).

motion equation: $$\frac{\partial V}{\partial t}+V\frac{\partial V}{\partial x}+g\frac{\partial H}{\partial x}+\frac{f}{2D}V|V|=0 \quad (1)$$

continuous equation: $$\frac{a^2}{g}\frac{\partial V}{\partial x}+V\left(\frac{\partial H}{\partial x}+\sin\alpha\right)+\frac{\partial H}{\partial t}=0 \quad (2)$$

$$C^+:\ \begin{cases}\frac{dH}{dt}+\frac{a}{gA}\frac{dQ}{dt}+\frac{af}{2gDA^2}Q|Q|=0\\ \frac{dx}{dt}=a\end{cases} \quad (3)$$

$$C^-:\ \begin{cases}\frac{dH}{dt}-\frac{a}{gA}\frac{dQ}{dt}-\frac{af}{2gDA^2}Q|Q|=0\\ \frac{dx}{dt}=-a\end{cases} \quad (4)$$

where V is the flow velocity, H is piezometric head, a is water hammer velocity, f is friction coefficient, D is pipeline diameter, α is the angle between the line and a horizontal surface of each section of the pipeline center, V and H respectively is the function of pipe length x and time t, A is pipe section area, Q is water flow in pipe section.

The difference network is constructed by the above simplified equation set, then the finite difference method is used to solve the problem. Fig.2 shows the characteristic line difference mesh. For Fig.2, the length of L pipeline is divided into N segment, the length of each segment is $\Delta x=L/N$, the time step of the differential network is $\Delta t=\Delta x/a$.

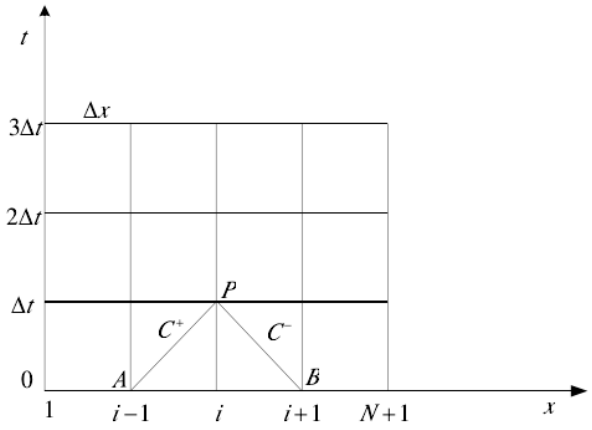

Fig.2 *x-t* characteristic line difference mesh

Diagonal AP satisfies the condition: $\Delta x = a\Delta t$, Diagonal BP satisfies the condition: $\Delta x = -a\Delta t$. The motion equation is calculated the line integral from A point to P point along the C^+ line; the continuous equation is calculated the line integral from B point to P point along the C^- line; and the calculation formula of integral is described as the formulas (5) and (6).

$$(H_P - H_A) + \frac{a}{gA}(Q_P - Q_A) + \frac{f}{2gDA^2}\int_A^P Q\,|Q|\,dx = 0 \tag{5}$$

$$(H_P - H_B) - \frac{a}{gA}(Q_P - Q_B) - \frac{f}{2gDA^2}\int_B^P Q\,|Q|\,dx = 0 \tag{6}$$

Finally, the correct processing and analog computation of boundary conditions for PSHU system in the transient process of the research and control are very important. The boundary conditions are a conduit or a terminal connected, including: upstream reservoir, upstream surge tank, series nodes, bifurcated pipe nodes, ball valve, PSHU, downstream surge tank and downstream reservoir. Besides surge tank and PSHU, the other boundary conditions as well as spiral case and tail pipe usually can be considered as pressure water pipeline.

2.2 Model of surge tank

There are many types of surge tank including impedance type, differential type and air cushion type ,in pumped storage power station which has been built. Depending on the actual situation of a pumped storage power station in China, the impedance surge tank is adopted by the PSHU system in this paper. The schematic diagram of the impedance surge tank is shown in Fig.3, From Fig.3, the impedance surge tank is connected with the water pipeline system through a small impedance orifice, which has the advantages of small volume and simple structure. And the corresponding basic equations can be described as formula (7) [29-31].

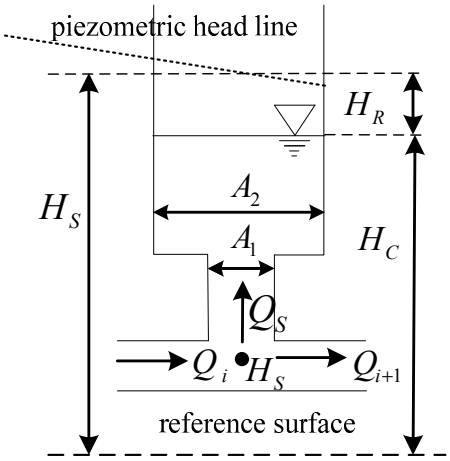

Fig.3 The schematic diagram of the impedance surge tank

$$\begin{cases} H_S = H_C + H_R \\ H_R = K_S |Q_S| Q_S \\ Q_S = A_2 \dfrac{dH_C}{dt} \\ K_S = \dfrac{K_R(Q_S)}{2gA_1^2} \end{cases} \tag{7}$$

where H_S, Q_S are the surge tank bottom pressure and flow, A_1 is the area of impedance orifice, H_C, A_2 are the elevation and area of surge tank, K_R is bottom orifice flow loss coefficient.

2.3 Model of PSHU

PSHU is composed of pump-turbine and generator, which are the key component of the PSHU system. At present, the pump-turbine modeling based on the characteristic curves has been widely used. In this paper, pump-turbine is be described as the torque function and flow function of guide vane opening, generator rotational speed and water head, shown as formula (8) [32]. The analytic expression of nonlinear functions of $f_m(\cdot)$ and $f_q(\cdot)$ are difficult to obtain. However, based on the characteristic curves (Fig.4), torque and flow of the pump-turbine at a certain time can be calculated by means of interpolation or nonlinear function fitting. In order to overcome obstacle of single input-multiple output during the process of interpolation calculating, Logarithmic-Curve-Projection method for the mathematical transformation of characteristic curves is adopted [33].

$$\begin{cases} m_t = f_m(y, x, h) \\ q = f_q(y, x, h) \end{cases} \tag{8}$$

Preprints (www.preprints.org) | NOT PEER-REVIEWED | Posted: 2 June 2017 doi:10.20944/preprints201706.0016.v1

Peer-reviewed version available at Energies 2017, 10, 911; doi:10.3390/en10070911

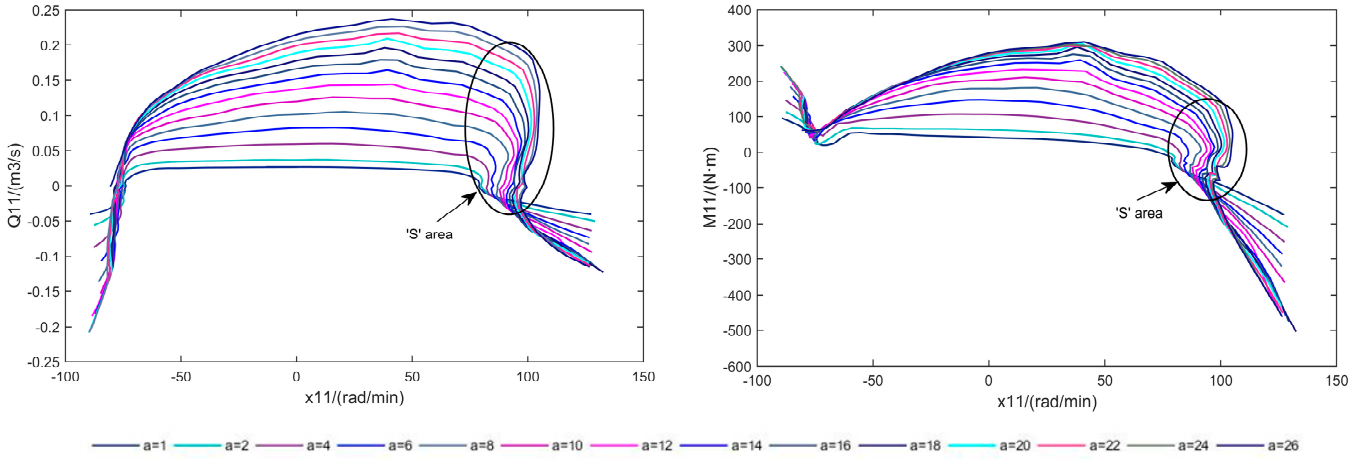

Fig.4 The characteristic curves of pump-turbine

In this paper, only the PSHU rotational speed change of standalone running at the isolated power grid is considered[34]. The dynamic equation of the synchronous generator when considering the load characteristics is simplified as the formula (9):

$$\frac{x(s)}{mt(s)-mg_0(s)}=\frac{1}{T_a s+e_g} \tag{9}$$

where x is the generator rotational speed, T_a is the inertial time constant of the generator, e_g is the adjusting coefficient of the generator, and mg_0 is the load disturbance which is representing the load change.

3. OGVCS problem formulation

The dynamic response characteristics of the unit and the hydraulic influence of the large fluctuation condition of the PSHU are analyzed under the condition of different guide vanes closing law. Considering two objectives of the increase of unit rotational speed and pressure appreciation of each node in the hydraulic unit, the optimal model of the guide vane closing law is established.

3.1 Objective function

3.1.1 rotational speed objective

Rising rotational speed is one of the main characteristics of the pumped storage unit when the load rejection or pump power off condition. In extreme cases, non optimal guide vane closing schemes and even lead to runaway phenomenon, huge centrifugal force rotating parts may cause mechanical damage, vibration and noise. The minimize rotational speed objective Obj_x of OGVCS problem can be expressed as follows:

$$Min\ Obj_x=\sum_{i=1}^{N_{pu}}(\max(x_i)-x_{r,i})/x_{r,i} \tag{10}$$

where N_{pu} is the number of units in a hydraulic unit, x_i is rotational speed of i unit during the transition process, $x_{r,i}$ is the rated rotational speed of the unit in stable condition.

3.1.2 water hammer pressure objective

In order to minimize the pressure of each hydraulic unit, comprehensive considering the volute end pressure, tail pipe inlet pressure and surge tank water level value, the water hammer pressure objective function Obj_{pre} is established as follows:

$$Min\ Obj_{pre} = w_P \sum_{i=1}^{N_{pu}} (P_{vol\_e,i} + P_{dra\_s,i}) + w_L (L_{sur\_up} + L_{sur\_down}) \tag{11}$$

where $P_{vol\_e,i}$, $P_{dra\_s,i}$ are the maximum value of the volute end pressure and tail pipe inlet pressure for i unit, L_{sur_up}, L_{sur_down} are the maximum value of the upstream surge tank and downstream surge tank, w_P, w_L are weight coefficient of water hammer pressure and water level in the surge tank.

3.2 Multiple constraints

The OGVCS problem should satisfy the following equality and inequality constraints:

(1) Rising rotational speed constraint

For calculation of regulation guarantee and transient process of PSHU system, there is a clear maximum constraint value constant_x for the rise value of rotational speed when all kinds of extreme cases occur.

$$Obj_{x,i} \le \text{constant}_x \tag{12}$$

(2) Limit of rotational speed fluctuation

In this paper, the limit of the times of rotational speed fluctuation is introduced in order to realize the good dynamic quality of the large fluctuation condition process.

$$\begin{cases} N_{xf} = \sum num(Obj_{x,i} \ge \text{constant}_{obj_{x_r}}) \\ N_{xf} \le \text{constant}_{xf} \end{cases} \tag{13}$$

where $\text{constant}_{obj_{x_r}}$ is rising rate constant for dynamic quality requirements, N_{xf} is fluctuation times, constant_{xf} is constraint constant of fluctuation times.

(3) Volute pressure constraint

The maximum corrected value and the pressure constraint of the volute inlet pressure considering the pressure fluctuation and the calculation error is described as follows:

$$\begin{cases} Pm_{vol\_s,i} = P_{vol\_s,i} + H_n \times 7\% + (P_{vol\_s,i} - P_{vol,i}) \times 10\% \\ Pm_{vol\_s,i} \le \text{constant}_{Pm_{vol\_s}} \end{cases} \tag{14}$$

where $P_{vol\_s,i}$, $P_{vol,i}$ and $Pm_{vol\_s,i}$ are maximum calculated value, initial value and maximum corrected value of volute inlet pressure for i unit, H_n is the net head, $\text{constant}_{Pm_{vol\_s}}$ is constraint constant of $P_{vol\_s,i}$.

(4) Draft tube inlet pressure constraint

$$\begin{cases} Pm_{dra\_s,i} = P_{dra\_s,i} - H_n \times 3.5\% - (P_{dra,i} - P_{dra\_s,i}) \times 10\% \\ Pm_{dra\_s,i} \ge 0\ m \quad \text{conventional condition} \\ Pm_{dra\_s,i} \ge -5\ m \quad \text{successive load rejection} \end{cases} \tag{15}$$

where $P_{dra\_s,i}$, $P_{dra,i}$ and $Pm_{dra\_s,i}$ are minimum calculated value, initial value and minimumcorrected value of draft tube inlet pressure for i unit.

(5) The surge water level limits

$$\begin{cases} L_{sur\_up} \le \text{constant}_{L_{sur\_up}} \\ l_{sur\_up} \ge \text{constant}_{l_{sur\_up}} \\ L_{sur\_down} \le \text{constant}_{L_{sur\_down}} \\ l_{sur\_down} \ge \text{constant}_{l_{sur\_down}} \end{cases} \quad (16)$$

where L_{sur_up} and l_{sur_up} are maximum and minimum value of surge water level of upstream surge tank, L_{sur_down} and l_{sur_down} are maximum and minimum value of surge water level of downstream surge tank, others are corresponding constraint constant.

(6) Speed governor oil velocity limit

If the PSHU guide vane closing time is too short, the governor control slope of the curve of high precision. In order to meet the so short closing time, servomotor oil speed must be large enough, which will cause major safety accidents. Therefore, this paper takes into account the limit factor of the slope control of the governor, and transforms it into the guide vane closing rate.

$$\Delta Y / t \le Y\_\max / Tr \quad (17)$$

where ΔY and $Y\_\max$ is change value and rated maximum value guide vane opening, t is guide vane closing time, Tr is minimum closing time limit.

4. Methodology of enhanced multi-objective BCGSA

4.1 Overview of BCGSA

BCGSA is improved from standard gravitational search algorithm (GSA) by introducing the strategies: P_{best}-G_{best}-guided movement, adaptive elastic-ball method and chemotaxis operator strategy. Then the specific processes of BCGSA are as follows.

Step 1: Initialization. Randomly initialize the agent of population position and velocity.

Step 2: Fitness calculation and information save. Calculate the fitness of agents according to their initial position, storing the current position of each agent $P_{best}(t)$ as the best record position of the agent and position of best agent $G_{best}(t)$ as the best position in global.

Step 3: Update best(t), worst(t), and M_i(t) for i = 1,2,. . .,N.

Step 4: Calculate the gravitational constant in the current iteration and acceleration for each agent.

Step 5: Update agents' velocity v_i^d and position x_i^d with formulas (18) and (19) [35].

$$v_i^d(t+1) = r_1 \cdot v_i^d(t) + a_i^d(t) + c_1 \cdot r_2 \cdot (P_{ibest}^d(t) - x_i^d(t)) + c_2 \cdot r_3 \cdot (G_{best}^d(t) - x_i^d(t)) \quad (18)$$

$$x_i^d(t+1) = x_i^d(t) + v_i^d(t) \quad (19)$$

where r_1, r_2 and r_3 are random variables in the range [0,1], c_1 and c_2 are learning genes in the range [0,2], $P_{ibest}(t)$ is the best position that i-th agent has ever suffered until time t, $G_{best}(t)$ is the global best position in the agents until time t.

Step 6: Judge whether the new position of the agent is beyond the boundary. Invoke the adaptive elastic-ball program (formula (20)) to handle the new position which is against the boundary. Besides, there are few rest agents against the boundary whose position will be reset by formula (21) [36].

$$\begin{cases} if\ x_i^d(t) > Ub(d),\ up = x_i^d(t) - Ub(d) \text{ and } x_i^d(t) = Ub(d) - \zeta \cdot up \\ if\ x_i^d(t) < Lb(d),\ down = Lb(d) - x_i^d(t) \text{ and } x_i^d(t) = Lb(d) + \zeta \cdot down \end{cases} \quad (20)$$

$$x_i^d(t) = rand \cdot (Ub(d) - Lb(d)) + Lb(d) \tag{21}$$

where ζ is the adaptive attenuation coefficient of reflective power, $Ub(d)$ and $Lb(d)$ are upper and lower boundary limit in the *d*-th dimension, respectively.

Step 7: Evaluate the fitness in accordance with the new position of each agent, storing position of best agent X^{best} and worst agent X^{worst} in the current iteration.

Step 8: Chemotaxis operator [37] is conducted for X^{best} and X^{worst}.

(1) Initialize parameters *Nc*, *Ns* and $C(i)$. Where *Nc* is the number of chemotaxis steps, *Ns* is the number of swim steps.

(2) Tumble. Generate a random vector $\Delta(i) \in R^D$ with each element $\Delta_d(i)$, $d = 1, 2, \cdots, D$, a random number on [−1,1].

(3) Move. Define unit length random direction $\phi(j)$ in *j*-th chemotaxis, then updates the best agent $X^{best} = [x_1^{best}, x_2^{best}, \cdots, x_d^{best}, \cdots, x_D^{best}]$ and worst agent $X^{worst} = [x_1^{worst}, x_2^{worst} \cdots, x_d^{worst}, \cdots, x_D^{worst}]$ according to formulas (22) and (23).

$$\phi(j) = \frac{\Delta(i)}{\sqrt{\Delta^T(i)\Delta(i)}} \tag{22}$$

$$x(i, j+1) = x(i, j) + C(i)\phi(j) \tag{23}$$

where X^{best} is the agent of the best fitness, X^{worst} is the agent of the worst fitness, $x(i, j)$ is the position of the *i*-th agent in the *j*-th chemotaxis.

(4) Swim. Compute fitness of obtained new agent $x(i, j+1)$, then compare $fitness(i, j+1)$ and $fitness(i, j)$. If the $fitness(i, j+1)$ is better, save the new agent as X_{new}^{best} or X_{new}^{worst} and start agent swimming, then let *m*=0 and repeat the formula (23) following this tumble direction until *m*=*Ns*; else let *n*=*Ns* directly, this is the end of the while statement.

(5) Repeat (1) to (4) until *Nc* reaches the stop criteria. And replace G_{best} and G_{worst} by X_{new}, only when X_{new}^{best} and X_{new}^{worst} is better.

Step 9: Compare the obtained fitness of a new position $x_i(t+1)$ with fitness of $P_{ibest}(t)$ and $G_{best}(t)$ while *i* changes from 1 to *N*. If $x_i(t+1)$ has a better fitness value, replace position of $P_{ibest}(t)$ and $G_{best}(t)$ by $x_i(t+1)$.

Step 10: Repeat Step 3 to Step 9 until the stop criteria reached.

4.2 The basic definition of multi-objective optimization problem

Generally, the multi-objective minimize optimization problem of n dimensions decision variable and m dimensions subunit objectives can be described as follows:

$$\begin{cases} y = \min \quad F(x) = \{\min f_1(x), \min f_2(x), ..., \min f_m(x)\} \\ subject \quad to \quad g_j(x) \geq 0 \quad (j = 1, 2, ..., J) \\ \qquad\qquad h_k(x) = 0 \quad (k = 1, 2, ..., K) \\ x = (x_1, x_2, ..., x_n) \end{cases} \tag{24}$$

where $[f_1, f_2, ..., f_m]$ are m dimensions of objective vectors, $F(x)$ is mapping function from decision space to object space, $g_j(x) \geq 0 \quad (j = 1, 2, ..., J)$ defines the J inequality constraints, $h_k(x) = 0 \quad (k = 1, 2, ..., K)$ defines the K inequality constraints, $x = (x_1, x_2, ..., x_n)$ is m dimensions decision variable space.

Due to the conflictive relationship among multiple subobjectives, a set of non-dominated solution exist rather than only one optimal solution. thus the key concept of Pareto optimality [38, 39] associated with the trade-off between conflictive objectives is adopted.

(1) Pareto dominance relation

X_f is a feasible solution set, x_1 and x_2 are feasible solutions, $[x_1, x_2] \in X_f$, if x_1 dominates x_2, note as $x_1 \succ x_2$, if and only if

$$\{\forall k = 1, 2, ..., m \mid f_k(x_1) \leq f_k(x_2)\} \wedge \{\exists l \in (1, 2, ..., m) \mid f_l(x_1) < f_l(x_2)\} \tag{25}$$

(2) Pareto optimal solution

For a given multi-objective optimal problem, if $x^* \in X_f$ is the Pareto optimal solution, if and only if

$$\neg \exists x \in X_f : x \succ x^* \tag{26}$$

(3) Pareto optimal solution set

The set of all Pareto optimal solutions is called the Pareto optimal solution set P^*.

$$P^* = \{x^* \mid \neg \exists x \in X_f : x \succ x^*\} \tag{27}$$

(4) Pareto optimal front

The Pareto optimal solution set corresponding to the objective vector value in the objective domain space is called the Pareto optimal front PF^*.

$$PF^* = \{F(x^*) = \{f_1(x^*), f_2(x^*), ..., f_m(x^*)\} \tag{28}$$

4.3 Enhanced multi-objective BCGSA

The BCGSA is based on the single objective optimization design, which does not have the ability to deal with multi-objective optimization problems. Therefore, based on the BCGSA, this section reconstructs the optimal structure and mechanism of solving multi-objective optimization problems.

4.3.1 Population reconstruction

For multi-objective optimization, the non inferior relationship analysis between individuals in a population becomes complicated and fuzzy, how the individuals are reasonable Pareto ordering to improve the computational efficiency and ergodicity of multi-objective optimization algorithm is essential. Therefore, this paper further introduced a fast non dominated sorting method, comprehensive analysis method, and the crowding-distance is calculated based on the individual level and at the basis of the new design method of the quality of individual crowding-distance calculation, and then complete the whole population structure reconstruction.

(1) Non-dominated sorting

In order to realize the distribution and diversity of population of the BCGSA algorithm in dealing with multi-objective optimization problems in this group, inspired by NSGA-II [20], the fast non dominated sorting method is applied to divide the population into a number of levels, the specific steps are as follows:

Step1: If any individual x_i^d is not dominant in the current population, the individual is Pareto non dominated, then its layer rank is 1, and all the individuals in the rank=1 constitute the Pareto optimal front.

Preprints (www.preprints.org) | NOT PEER-REVIEWED | Posted: 2 June 2017 doi:10.20944/preprints201706.0016.v1

Peer-reviewed version available at Energies 2017, 10, 911; doi:10.3390/en10070911

Step2: In the whole population, the individuals of rank=1 are excluded; then repeat Step1 until obtain the individual solution set of the second layer, and the individual attributes of the rank=2 are given.

Step3: By analogy, repeat Step 2 until the completion of the entire population of non dominated sort. Assuming that the population size is 7, the objective number is 2, and the layering schematic is shown in Fig.5.

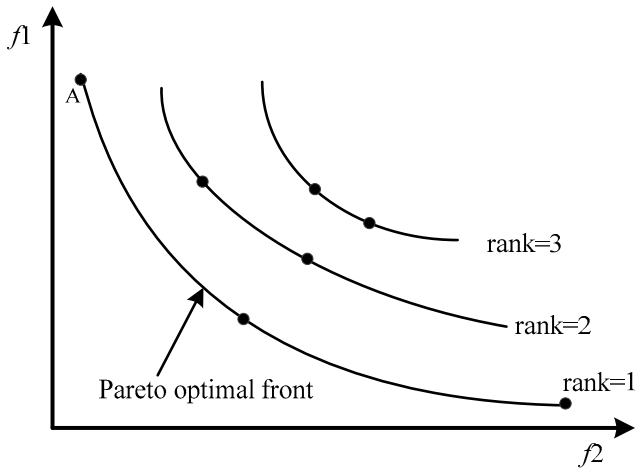

Fig.5 The layering schematic of population

(2) Crowding-distance calculation

Further, another attribute of each layer individual is given a "crowding-distance". Crowding-distance [20] is an important indicator for evaluating the density distribution of the non dominated solutions, which can be used to evaluate the relative distance between a single individual and its surroundings. And, the aggregation density of non inferior individuals with small crowding distance. The formula for calculating the crowding-distance is as follows:

$$\Gamma[p]_{distance}=\begin{cases}\sum_{l=1}^{L}[(f_{p-1,l}-f_{p+1,l})/(f_l^{\max}-f_l^{\min})]^2, p\in[2,Nr-1]\\ \sum_{l=1}^{L}2[(f_{1,l}-f_{2,l})/(f_l^{\max}-f_l^{\min})]^2, p=1\\ \sum_{l=1}^{L}2[(f_{Nr-1,l}-f_{Nr,l})/(f_l^{\max}-f_l^{\min})]^2, p=Nr\end{cases} \tag{29}$$

where $\Gamma[p]_{distance}$ is crowding-distance of individual p, $f_{p,l}$ is fitness value of objective l of individual p, L is the number of objective, $f_l^{\max}$ and $f_l^{\min}$ are maximum and minimum fitness values for individuals in each layer of the L dimensional objective.

Thus, each individual consists of two attributes: the layer number and the crowding-distance. Depending on these two attributes can be defined between individual preference relations. i is superior to j, if and only if:

$$\begin{cases}rank(i)<rank(j)\\ rank(i)=rank(j),\Gamma[i]_{distance}>\Gamma[j]_{distance}\end{cases} \tag{30}$$

(3) Individual quality calculation

For EMOBCGSA, the quality of the individual cannot be calculated based on the value of the objective function, but it is obtained by the rank of the non dominated layer number. For l objective functions of MOO, the calculation process of individual quality is as follows:

Step1: In the rank=1, the fitness values of the individuals with the smallest value of l objective functions and the maximum crowding-distances are set to 1, and the fitness value of other individuals is 2.

Step2: In the rank=2, set all the individual fitness values to 3.

Step3: Repeat step 2, individual fitness value of $rank \geq 3$ is set to $(rank+1)$, thus completing all layers of individual fitness assignment.

Step4: Calculate individual quality by formula (31).

$$\begin{cases} m_i(t) = \dfrac{fit_i(t) - worst(t)}{best(t) - worst(t)} \\ M_i(t) = \dfrac{m_i(t)}{\sum_{j=1}^{N} m_j(t)} \end{cases} \tag{31}$$

4.3.2 Multi-objective adaptive chemotaxis operation

For multi-objective adaptive chemotaxis operation, the selection of G_{best} and G_{worst} is the key to speed up the convergence of EMOBCGSA. In order to avoid the premature and maintain the diversity of the population, the concept of constraint violation, as shown in formula(32), is introduced in the selection process. Combined with individual crowding-distance, calculate the probability of individual selection in rank=1 and rank=max, as shown in formula (33). By means of formulas (32) and (33) to adaptive calculate the probability of individual selection, then the tracking targets (G_{best} and G_{worst}) of multi objective chemotaxis operation are determined by the roulette wheel method.

$$voilation_s = \begin{cases} \sum_{ic=1}^{nc} \dfrac{value_{ic} - Lu_{ic}}{Lu_{ic} - Ld_{ic}} & value_{ic} \geq Lu_{ic} \\ \sum_{ic=1}^{nc} \dfrac{Ld_{ic} - value_{ic}}{Lu_{ic} - Ld_{ic}} & value_{ic} \leq Ld_{ic} \end{cases} \tag{32}$$

$$p_s = \begin{cases} Sp1 \times \dfrac{1/voilation_s}{\sum_{v=1}^{N_v} 1/voilation_v}, & if \quad voilation_s > \varepsilon \\ Sp2 \times \dfrac{\Gamma[s]_{distance}}{\sum_{d=1}^{N_d} \Gamma[d]_{distance}}, & otherwise \end{cases} \tag{33}$$

where $voilation_s$ is constraint violation of individual s, $value_{ic}$ constraint value is of constraint ic, Lu_{ic} and Ld_{ic} are the upper and lower limits of constraint ic, nc is the number of constraints; p_s is selection probability of s, ε is feasible margin of constraint failure depth evaluation (if $voilation_s > \varepsilon$, and individual s is infeasible solution), N_v and N_d are number of infeasible solutions and feasible solutions, $Sp1$ and $Sp2$ are initial selected probability constant of infeasible solution and feasible solution.

4.3.3 Multi-objective velocity update strategy

For velocity update formula (18) of EMOBCGSA, G_{best} and P_{best} need to be redefined when dealing with multi objective problems. The selection mechanism of G_{best} has been detailedly introduced in section 4.3.2, and $P_{ibest}^{d}(t)$ is the location of the optimal memory of the individual i on the d dimension of the t generation. The selection method of P_{best} can be carried out according to the formula (30).

4.3.4 The update and maintenance of elite archive set

The elite archive set (EAS) is used to store the non dominated solutions obtained during EMOBCGSA evolution, and provide guidance for the evolution of a population. In the actual operation of the algorithm, the newly generated individual np_s^g and the original individual p_s^g are added to EAS when np_s^g and p_s^g are mutually reciprocal domination. EAS update and maintenance strategies are as follows(NQ is the capacity of EAS):

(1) If the current capacity of EAS is zero, the elite candidates are added directly to the EAS.

(2) If the EAS is not empty, and the elite candidate is not dominated by any elite individual in the original EAS, the elite candidate is added to the EAS. At the same time, the initial elite individual who is dominated by the candidate elite is removed from the EAS.

(3) If the number of elite individuals stored in EAS has exceeded NQ, the EliteSet truncation method is used to maintain it.

All the individuals will be selected by the non dominated sorting, and the first NQ individuals with larger crowding-distance will be stored in EAS, and the redundant individuals will be removed from there.

5. Numerical experiments and analysis

5.1 Proposed EMOBCGSA approach for OGVCS problem

Depending on the mathematical description of the optimization objectives and constraints, OGVCS is a multi-objective optimization problem with multiple variables and multiple nonlinear constraints. The objectives and constraints involve a lot of hydraulic and mechanical factors, so it is urgent to get an efficient algorithm to solve the model. In this section, the procedure of the proposed EMOBCGSA for solving OGVCS problem with complex constraints is described, and corresponding constraints-handling strategy will be discussed later. The generalized procedure can be given in follows.

5.1.1 Population initialization

At present, the common guide vane closing mode is straight line closure, two segment type broken line closure and three segment delay broken line closure. Because the governor of PSHU does not have the function of delay in the pump condition, this paper does not consider the three segment closing law. Fig.6 shows the schematic diagram of the straight line closure and the broken line closure.

Preprints (www.preprints.org) | NOT PEER-REVIEWED | Posted: 2 June 2017 doi:10.20944/preprints201706.0016.v1

Peer-reviewed version available at Energies 2017, 10, 911; doi:10.3390/en10070911

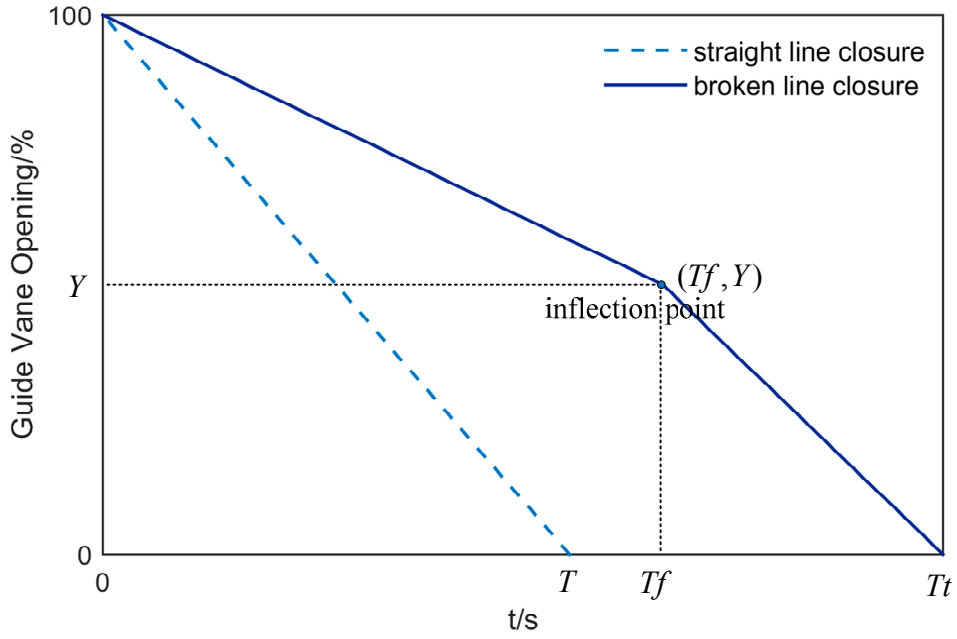

Fig.6 Schematic diagram of the straight line closure and the broken line closure

From Fig.6, T and $[Tf, Y, Tt]$ are the decision variables of two kinds of closing law, respectively. Take the broken line closure as an example, assuming that the optimized 'single tube-N_{PT} units' type PSHU system, the individual a can be constructed as matrix U_a with $3\times N_{PT}$. U_a is described as formula (34), Np is the size of population. Individuals can be randomly initialized by formula (35).

$$U_a = \begin{bmatrix} Tf_{1,1} & Tf_{1,2} & \cdots & Tf_{1,n} & \cdots & Tf_{1,N_{PT}} \\ Y_{2,1} & Y_{2,2} & \cdots & Y_{2,n} & \cdots & Y_{2,N_{PT}} \\ Tt_{3,1} & Tt_{3,2} & \cdots & Tt_{3,n} & \cdots & Tt_{3,N_{PT}} \end{bmatrix}, \quad a = 1,2,\ldots,Np \tag{34}$$

$$\begin{cases} Tf_{1,n} = Tf_{1,n}^{\min} + rand(0,1)\times(Tf_{1,n}^{\max} - Tf_{1,n}^{\min}) \\ Y_{1,n} = Y_{1,n}^{\min} + rand(0,1)\times(Y_{1,n}^{\max} - Y_{1,n}^{\min}) \\ Tt_{1,n} = Tt_{1,n}^{\min} + rand(0,1)\times(Tt_{1,n}^{\max} - Tt_{1,n}^{\min}) \end{cases} \quad n = 1,2,\ldots,N_{PT} \tag{35}$$

where $Tf_{1,n}^{\max}$ and $Tf_{1,n}^{\min}$ are the upper and lower limits of Tf, $Y_{1,n}^{\max}$ and $Y_{1,n}^{\min}$ are the upper and lower limits of Y, $Tt_{1,n}^{\max}$ and $Tt_{1,n}^{\min}$ are the upper and lower limits of Tt.

5.1.2 Constraints-handling strategy

In this section, based on the concept of constraint violation, a novel constraints-handling strategy with eliminating and local search based on violation ranking are used to balance various hydraulic and mechanical constraints is proposed to deal with OGVCS problem. The speed governor oil velocity limit of the governor can be dealt with after the initialization and update of the individual, and the additional constraint is to judge whether the individual has violated the constraint condition after the OGVCS problem is solved. Therefore, constraints-handling strategy can be divided into two parts: pre repair and post repair.

(1) Pre repair

Pre repair is mainly aimed at the speed governor oil velocity constraints. The processing steps are as follows:

Step 1: For individual i, calculate the closing rate for each segment $\Delta Y/t$, judge the relationship between $\Delta Y/t$ with the rated closing rate $Y\_\max/Tr$.

Step 2: If $\Delta Y/t > Y\_\max/Tr$, the closing rate of the guide vanes assigned to this segment is $Y\_\max/Tr$, reverse calculation closing time t_new, then replace t with t_new.

Step 3: Repeat step 1 and step 2, until all of the individuals constraints have been repaired.

(2) Post repair

The OGVCS problem is solved by the individuals who have been pre repaired. According to the calculation value of the transient process of each hydraulic unit of PSHU system and formula (32), calculate the total amount of constraint violation $voilation_i$. If $voilation_i \neq 0$, according to eliminate and local search strategy based on violation ranking for post repair, detailed steps are as follows:

Step 1: Do a descending sort for individuals of $voilation_i \neq 0$.

Step 2: Introduce coefficient Cv of constraint violation, if $voilation_i < Cv$, start local iterative search procedure; randomly generated Δy_i, and position of inflection point of two segment type broken line closure is updated to $Y_i + \Delta y_i$, calculate the OGVCS problem; repeat the above local iterative search procedure until $voilation_i = 0$ or meet required local search steps.

Step 3: Repeat step 1, complete local iterative search for individuals who are $voilation_i < Cv$, eliminate individuals who is $voilation_i \neq 0$.

5.1.3 Outline of EMOBCGSA for solving OGVCS problem

The process of OGVCS problem solving with EMOBCGSA is described as follows, and the flowchart is illustrated in Fig.7.

Step 1: Set guide vane closing mode and corresponding parameters; initialize the control parameters $[NQ, Np, G_{\max}, G_0, \beta, c_1, c_2, Nc, Ns]$ of the EMOBCGSA, set the evolutionary current algebra $g = 1$.

Step 2: According to formula (34) and (35) construct and initialize individuals of a population.

Step 3: Complete the constraints pre repair of individuals; simulation solving the OGVCS problem, Obj_x and Obj_{pre} are calculated by formula (10) and (11) respectively; complete the constraints post repair; the non dominated sorting of the population was conducted to determine the number of layer and crowding-distance of the population, and all the non dominated individuals of the rank=1 layer to meet the constraints were added to EAS.

Step 4: Population evolution.

(1) Population reconstruction. Calculate $G(t)$, $P_{ibest}(t)$ and $G_{best}(t)$, the $M_i(t)$ of the individual is calculated by the number of ranks and crowding-distance.

(2) Multi-objective chemotaxis operation. Determine the tracking target $G_{best}(t)$ and $G_{worst}(t)$ of multi-objective chemotaxis operation, update $G_{best}(t)$ and $G_{worst}(t)$ of population by chemotaxis operation.

(3) Individual updates. Calculating the resultant gravity force and update velocity of individual; updating the individual based on the multi-objective velocity update strategy.

Step 5: If $g < G_{\max}$, set $g = g + 1$, repeat Step 3 and Step 4, and update and maintenance of EAS; otherwise output the current EAS as the Pareto optimal front, OGVCS problem calculation completed.

Preprints (www.preprints.org) | NOT PEER-REVIEWED | Posted: 2 June 2017 doi:10.20944/preprints201706.0016.v1

Peer-reviewed version available at Energies 2017, 10, 911; doi:10.3390/en10070911

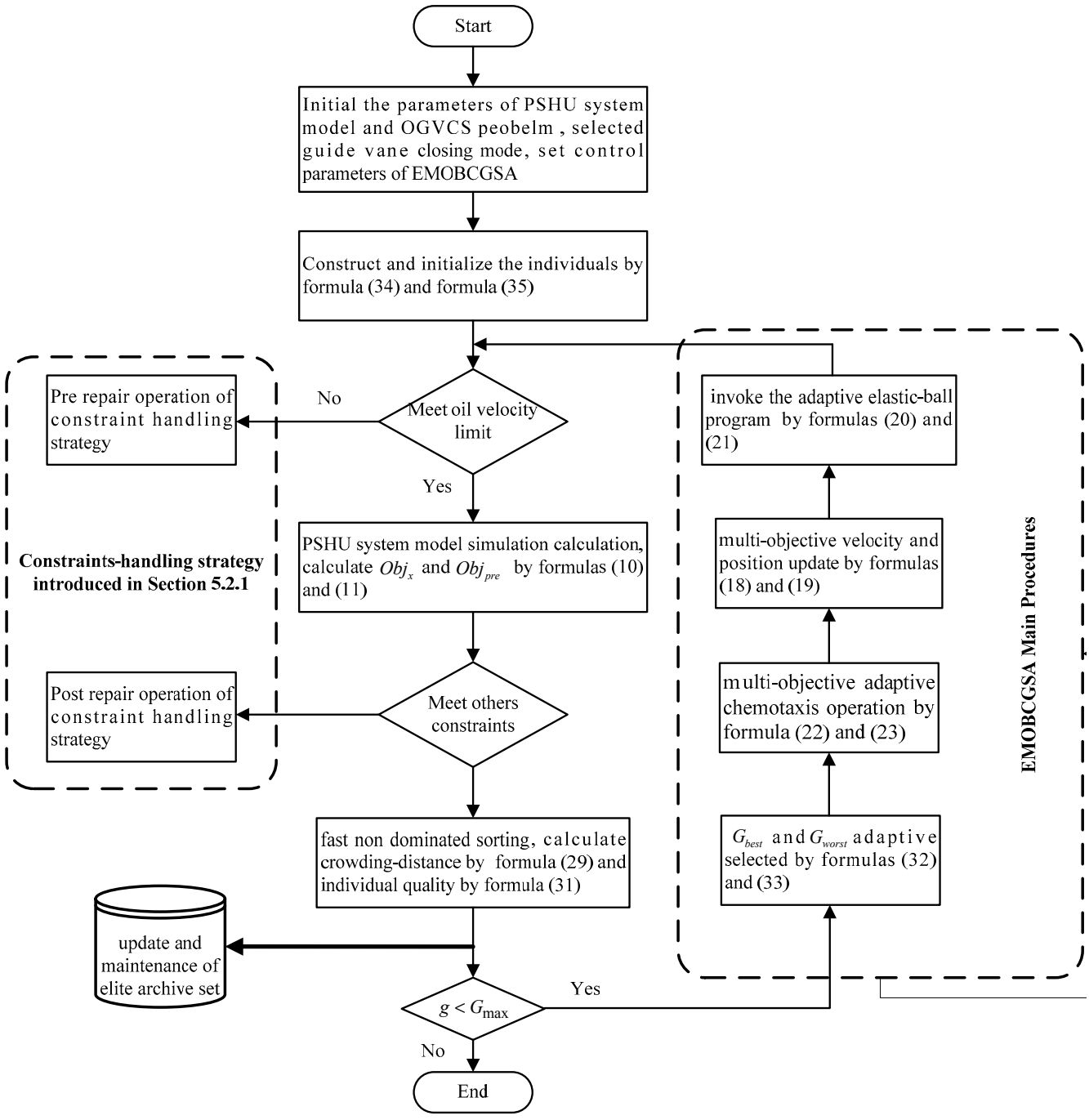

Fig.7 The flowchart of EMOBCGSA for solving OGVCS problem

5.2 Experiments study and anaysis

5.2.1 Experiment scenarios and parameters setting

In this section, the 'single tube-double units' type PSHU system model is constructed to verify the feasibility and effectiveness of EMOBCGSA for solving the OGVCS problem. The model parameters are calculated on the basis of the actual parameters of a Chinese pump storage plant (PSP). The actual physical parameters of the PSP and PSHU are given in Table 1. The flow and torque characteristic curves of the TPV32-LJ-385 pump-turbine is shown in Fig.4. Additionally, the

simulation conditions of the experiment are set as shown in Table 2, four scenarios of guide vane closing modes are used for model validation experiments.

Table 1 Actual physical parameters of the PSP and PSHU

runner diameter (m)	rated speed(rad/min)	rated flow (m^3/s)	rated head/lift（m）	rated load (MW)
3.85	500	62.09	540	306

Table 2 Setting and description of system simulation operating conditions

condition	upper reservoir water level（m）	lower reservoir water level（m））	load change	detailed description
load rejection	735.45	181	100%→0	Upper: check the flood level. Head: Near the rated head. Output: rated. Condition:sudden load rejection. Guide vane: normally closed
pump outage	735.45	184.11	100%→0	Upper: dead water level Lift: lowest. Iutput: rated. Condition: outage of maximum pumping flow. Guide vane: normally closed.

Four scenarios of guide vane closing mode are described as follows:scenario 1, straight line closure, the same guide vane closing time of two units; scenario 2, straight line closure, the different guide vane closing time of two units; scenario 3, two segment type broken line closure, the same guide vane closing time of two units; scenario 4, two segment type broken line closure, the different guide vane closing time of two units. In this work, the parameters set: $NP=100$, $NQ=30$, $G_{\max}=200$, $G_0=30$, $\beta=10$, $c_1=c_2=2.0$, $Nc=5$, $Ns=5$. Also, in order to overcome the randomness of three heuristic algorithms, 30 trials are tried and average results are obtained.

5.2.2 Load rejection condition

With simulation operating conditions and parameters setting in Section 5.2.1, the proposed EMOBCGSA is used to solve the OGVCS problem with considering various hydraulic and mechanical constraints. To testify the effectiveness of EMOBCGSA, it is compared with some excellent algorithms, i.e., NSGA-II and MOPSO. The distributions of Pareto optimal schemes of four scenarios in EAS obtained by different algorithms are shown in Fig.8, and the objective function values of these schemes are given in Table 3. As can be noted from Fig. 8, compared with the NSGA-II and MOPSO, EMOBCGSA showed better convergence and distribution of the elite non dominated solutions in EAS obtained, the non dominated solutions closer to the true Pareto optimal front. Meantime, these non dominated solutions dominate that of the other two algorithms, and have fewer objective conflicts. Schemes of EMOBCGSA are distributed more uniformly and widely on the Obj_x

Preprints (www.preprints.org) | NOT PEER-REVIEWED | Posted: 2 June 2017 doi:10.20944/preprints201706.0016.v1

Peer-reviewed version available at Energies 2017, 10, 911; doi:10.3390/en10070911

and Obj_{pre}, which proves that the method proposed in this paper can balance and optimize both the rising rate of rotation and the water hammer pressure at the same time.

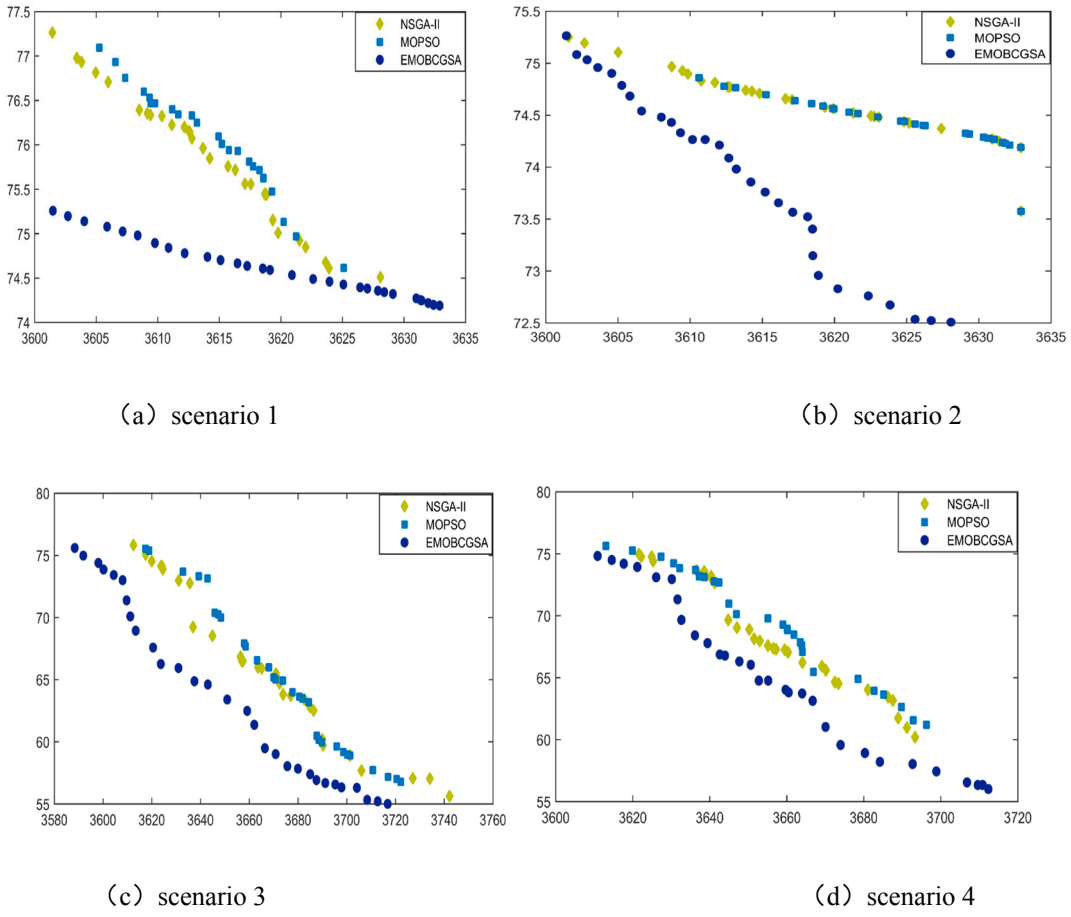

（a）scenario 1 （b）scenario 2

（c）scenario 3 （d）scenario 4

Fig.8 The Pareto front obtained by different algorithms

Comparative analysis of EMOBCGSA Pareto non dominated set by the four scenarios, as shown in Fig.9. From Fig.9, it is clear that the non dominated solution set obtained in scenario 3 is more close to the true Pareto optimal front, and has the sets of minimum water hammer pressure, lowest rising rotational speed and the most balanced of the two objectives. Therefore, under load rejection condition, the closure of scenario 3 can make the PSHU system operation safer and more stable. In Table 3, the Obj_{pre} is presented in an ascending order and Obj_x is presented in a descending order. In comparison to the two objectives obtained by different scenarios, the proposed scenario 3 can reduce 13.2 mH_2O, 13.1 mH_2O and 13.6 mH_2O at best Obj_{pre}, 19.17%, 17.49% and 1.01% at best Obj_x. Based on the above results analysis, the proposed method can get the optimal solution set, which makes the PSHU running safely and stably, and the water diversion system has the smallest fluctuation, which provides the best decision space for the decision maker.

Preprints (www.preprints.org) | NOT PEER-REVIEWED | Posted: 2 June 2017 doi:10.20944/preprints201706.0016.v1

Peer-reviewed version available at Energies 2017, 10, 911; doi:10.3390/en10070911

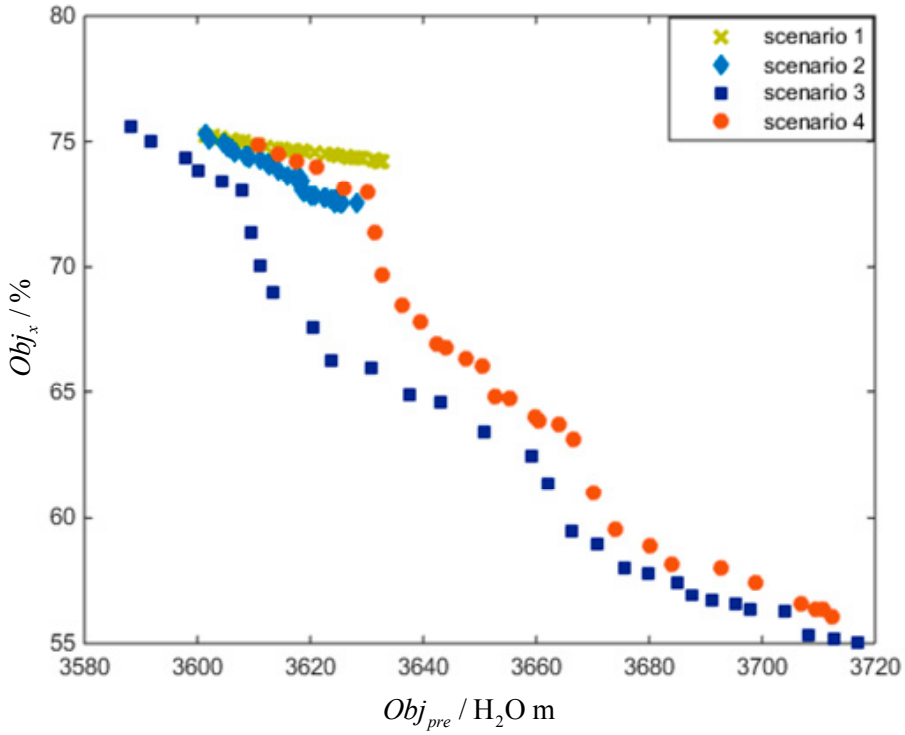

Fig.9 The Pareto front obtained by different scenarios under load rejection

Table 3 The detailed Pareto optimal schemes obtained of EMOBCGSA by different scenarios under load rejection

scheme	scenario 1		scenario 2		scenario 3		scenario 4	
	Obj_{pre}	Obj_x	Obj_{pre}	Obj_x	Obj_{pre}	Obj_x	Obj_{pre}	Obj_x
1	3601.5	75.26	3601.4	75.27	3588.3	75.60	3610.9	74.83
2	3602.7	75.19	3602.1	75.08	3591.9	74.99	3614.5	74.51
3	3604	75.14	3604.6	74.90	3598	74.38	3617.7	74.21
4	3605.9	75.08	3605.3	74.79	3600.2	73.87	3621.1	73.95
5	3607.2	75.03	3605.8	74.68	3604.3	73.43	3626.1	73.11
6	3608.4	74.98	3606.6	74.54	3608	73.02	3630.1	72.95
7	3609.8	74.89	3608.7	74.43	3609.6	71.38	3631.6	71.34
8	3610.9	74.84	3608.9	74.43	3611.2	70.08	3632.6	69.68
9	3612.2	74.78	3609.2	74.36	3613.4	68.96	3636.1	68.42
10	3614	74.74	3611.1	74.26	3620.6	67.60	3639.4	67.79
11	3615.1	74.70	3612.4	74.11	3623.6	66.27	3642.6	66.88
12	3616.5	74.67	3612.7	74.09	3631	65.94	3643.9	66.79
13	3617.3	74.64	3614.2	73.86	3637.5	64.87	3647.6	66.30
14	3618.5	74.61	3616.1	73.66	3643	64.62	3650.6	66.04
15	3619.1	74.58	3617.1	73.57	3650.9	63.41	3652.7	64.77
16	3620.9	74.53	3618.1	73.52	3659.1	62.48	3655.2	64.76
17	3622.6	74.49	3618.5	73.40	3662	61.38	3659.7	64.03
18	3624	74.46	3618.5	73.15	3666.4	59.48	3660.5	63.83
19	3625	74.43	3618.7	73.05	3670.8	59.01	3663.9	63.74
20	3626.4	74.40	3618.9	72.96	3675.7	58.06	3666.7	63.14
21	3627	74.38	3620.2	72.83	3679.9	57.83	3670.1	61.03
22	3627.9	74.36	3620.9	72.81	3685	57.41	3674	59.57

Preprints (www.preprints.org) | NOT PEER-REVIEWED | Posted: 2 June 2017 doi:10.20944/preprints201706.0016.v1

Peer-reviewed version available at Energies 2017, 10, 911; doi:10.3390/en10070911

23	3628.4	74.34	3622.3	72.76	3687.5	56.94	3680.3	58.92
24	3629.1	74.32	3622.7	72.74	3691.2	56.69	3684.1	58.21
25	3630.9	74.27	3623.8	72.67	3695.3	56.59	3692.7	58.05
26	3631.3	74.25	3624.2	72.65	3697.9	56.35	3698.8	57.45
27	3631.4	74.25	3624.3	72.56	3704.2	56.30	3706.8	56.57
28	3631.9	74.22	3625.3	72.55	3708.4	55.33	3709.6	56.35
29	3632.4	74.20	3625.6	72.53	3712.7	55.22	3710.8	56.34
30	3632.9	74.19	3628.1	72.51	3716.8	55.02	3712.3	56.03

Additionally, in order to verify availability of the proposed constraints-handling strategy, best Obj_{pre} and Obj_x schemes of scenario 3 is taken as the compromise schemes in our study. The simulation results of PSHU transition process and the corresponding index values are shown in Fig.10, Table 4 and Table 5. It can be seen clearly from the chart and tables that the transition process of the corresponding scheme satisfies the above definition of multiple constraints and has a good dynamic response process of PSHU.

Table 4 The index values of minimum Obj_x and Obj_{pre} schemes of scenario 3 (I)

schemes	volute end		Obj_x	draft inlet		volute end		Obj_x	draft inlet	
	min	max	%	min	max	min	max	%	min	max
	1#					2#				
minimum Obj_x	549.3	896.6	27.5	69.32	99.26	549.3	896.6	27.5	69.32	99.26
minimum Obj_{pre}	509.6	817.9	37.8	69.33	98.66	509.6	817.9	37.8	69.33	98.66

Table 5 The index values of minimum Obj_x and Obj_{pre} schemes of scenario 3 (II)

schemes	upstream surge water level			downstream surge water level		
	initial	min	max	initial	min	max
minimum Obj_x	734.53	731.1	746.2	182.63	166.9	189.3
minimum Obj_{pre}	734.52	733.34	746.8	182.64	168.13	189.1

Preprints (www.preprints.org) | NOT PEER-REVIEWED | Posted: 2 June 2017 doi:10.20944/preprints201706.0016.v1

Peer-reviewed version available at Energies 2017, 10, 911; doi:10.3390/en10070911

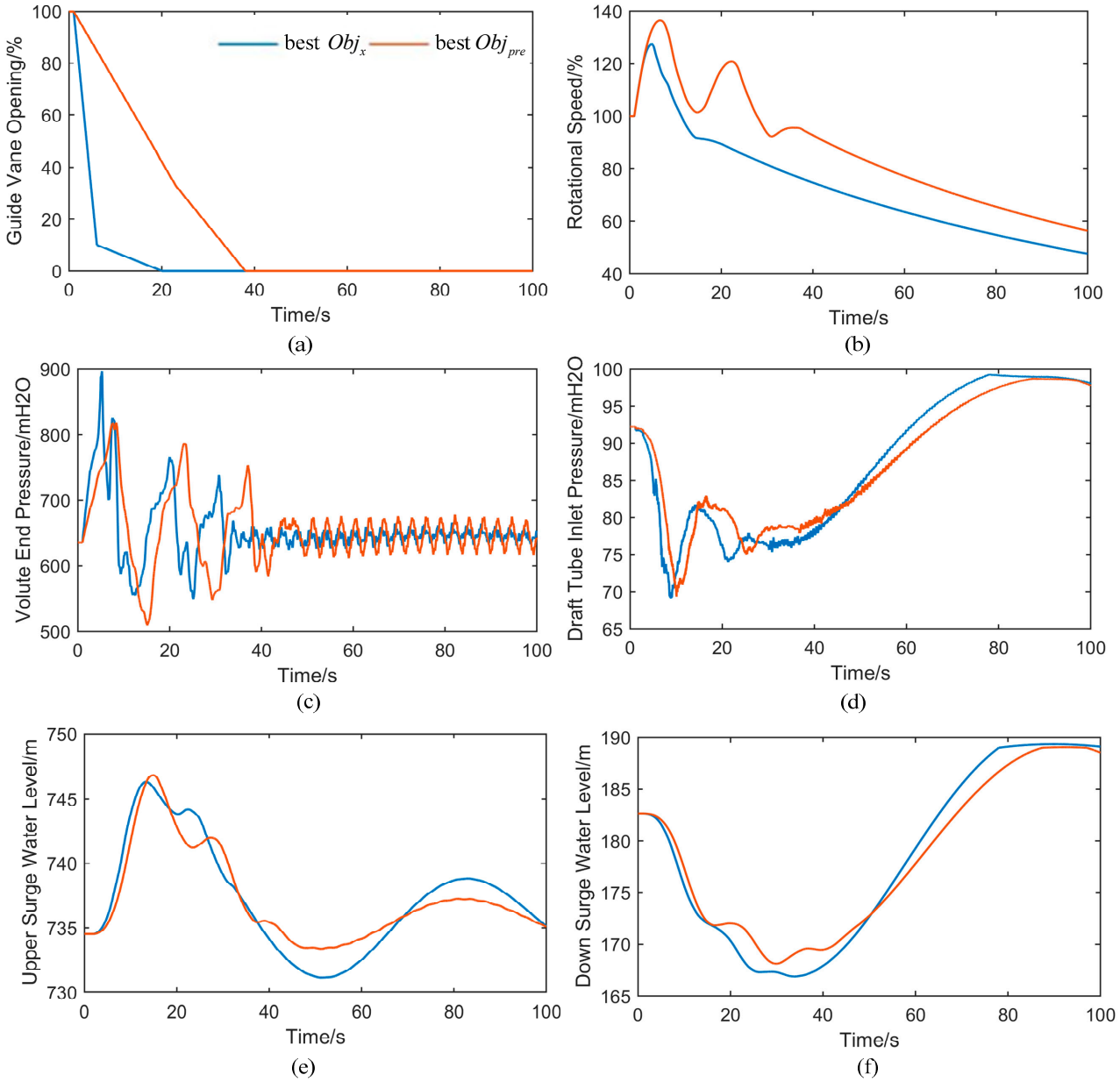

Fig.10 The transient process of minimum Obj_x and Obj_{pre} schemes of scenario 3

5.2.3 pump outage condition

Under pump outage condition, comparative analysis of EMOBCGSA Pareto non dominated set by the four scenarios, as shown in Fig.11. From Fig.11, it is evident that the non dominated solution set obtained in scenario 4 is more close to the true Pareto optimal front, and has the sets of best Obj_{pre}, Obj_x and the most balanced of the two objectives. In Table 6, the Obj_{pre} is presented in an ascending order and Obj_x is presented in a descending order, and select schemes at the inflection point of Pareto optimal front by four scenarios for the comparative analysis (15 scheme in scenario 1, 14 scheme in scenario 2, 17 scheme in scenario 3, 22 scheme in scenario 4). The simulation results of PSHU transition process under pump outage condition and the corresponding index values are presented in Fig.12, Table 7 and Table 8. From guide vane closing laws of Fig.12 (a) and index values, the draft inlet pressure increases at first and then decreased and stabilized; rotational speed extreme value depends on the guide vane closing time, if the closing time is short, the unit will only run in the pump and pump brake operating area, and be no rotating speed reversal phenomenon. Therefore,

Preprints (www.preprints.org) | NOT PEER-REVIEWED | Posted: 2 June 2017 doi:10.20944/preprints201706.0016.v1

Peer-reviewed version available at Energies 2017, 10, 911; doi:10.3390/en10070911

the closing time of the guide vane is extremely important to the transient process of the PSHU under pump outage condition.

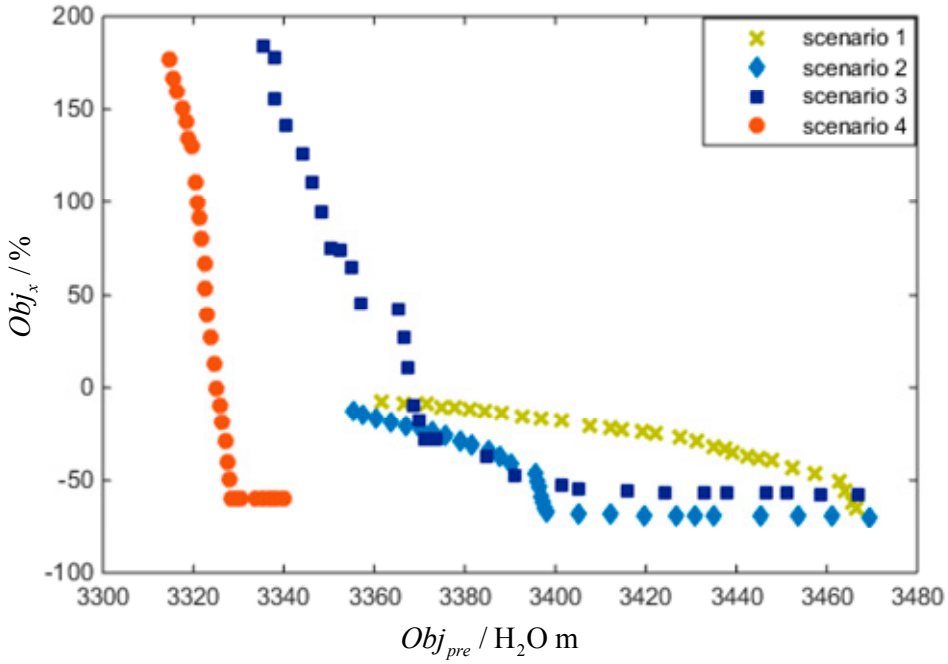

Fig.11 The Pareto front obtained of EMOBCGSA by different scenarios under pump outage

Table 6 The detailed Pareto optimal schemes obtained of EMOBCGSA by different scenarios under pump outage

scheme	scenario 1		scenario 2		scenario 3		scenario 4	
	Obj_{pre}	Obj_x	Obj_{pre}	Obj_x	Obj_{pre}	Obj_x	Obj_{pre}	Obj_x
1	3361.6	-7.293	3355.3	-13.15	3335.4	183.9	3314.7	177.4
2	3366.4	-8.185	3357.4	-14.71	3337.9	178.2	3315.5	166.7
3	3371.6	-9.177	3360.2	-16.81	3338.1	155.6	3316.5	159.9
4	3374.7	-10.29	3363.8	-19.29	3340.3	140.9	3317.5	150.5
5	3377.6	-11.11	3366.8	-20.98	3344.3	126.1	3318.3	143.5
6	3381	-12.01	3370.2	-22.67	3346.4	110.9	3318.9	134.6
7	3384.4	-13.08	3372.8	-24.30	3348.1	94.90	3319.5	129.8
8	3388.2	-14.17	3375.5	-25.85	3350.3	74.55	3320.5	110.4
9	3392.8	-15.66	3379.1	-28.80	3352.6	73.83	3320.8	99.44
10	3396.7	-16.87	3381.6	-31.07	3355.1	65.14	3321.2	91.33
11	3401.3	-18.29	3385.3	-34.20	3357.2	45.14	3321.6	79.87
12	3407.8	-20.45	3387.6	-37.63	3365.2	41.95	3322.4	66.53
13	3412.1	-21.65	3390.1	-41.09	3366.4	26.95	3322.8	53.77
14	3414.6	-22.60	3395.5	-46.54	3367.6	10.41	3323.2	39.78
15	3419.4	-24.13	3396	-50.54	3368.8	-9.210	3323.8	26.65
16	3422.1	-25.05	3396.4	-53.54	3370	-17.39	3324.8	13.22
17	3427.7	-27.40	3396.8	-58.54	3371.2	-27.95	3325.2	0
18	3431.3	-29.40	3397.2	-61.54	3373.7	-28.17	3326	-9.580
19	3435.1	-32.39	3397.6	-64.54	3384.6	-37.42	3326.4	-18.38
20	3437.4	-33.53	3397.9	-66.65	3391	-47.83	3327.2	-29.40
21	3439	-34.84	3404.9	-68.17	3401.3	-52.89	3327.6	-40.40
22	3442.7	-37.02	3412	-68.33	3405.2	-54.67	3328	-49.40
23	3445.1	-37.82	3419.5	-68.53	3416.1	-55.78	3328.4	-59.38

Preprints (www.preprints.org) | NOT PEER-REVIEWED | Posted: 2 June 2017 doi:10.20944/preprints201706.0016.v1

Peer-reviewed version available at Energies 2017, 10, 911; doi:10.3390/en10070911

24	3447.9	-39.68	3426.9	-68.64	3424.1	-56.17	3329.6	-59.40
25	3452.6	-42.96	3431	-68.76	3433	-56.52	3330.4	-59.42
26	3457.6	-46.25	3435	-68.84	3437.7	-56.68	3334	-59.44
27	3462.9	-50.36	3445.2	-68.92	3446.8	-56.90	3335.6	-59.46
28	3464.1	-55.95	3453.5	-69.03	3451.2	-57.01	3337.2	-59.46
29	3465.7	-61.56	3461	-69.14	3458.6	-57.21	3338.4	-59.47
30	3466.7	-64.87	3469.3	-69.75	3467.1	-57.49	3340	-59.48

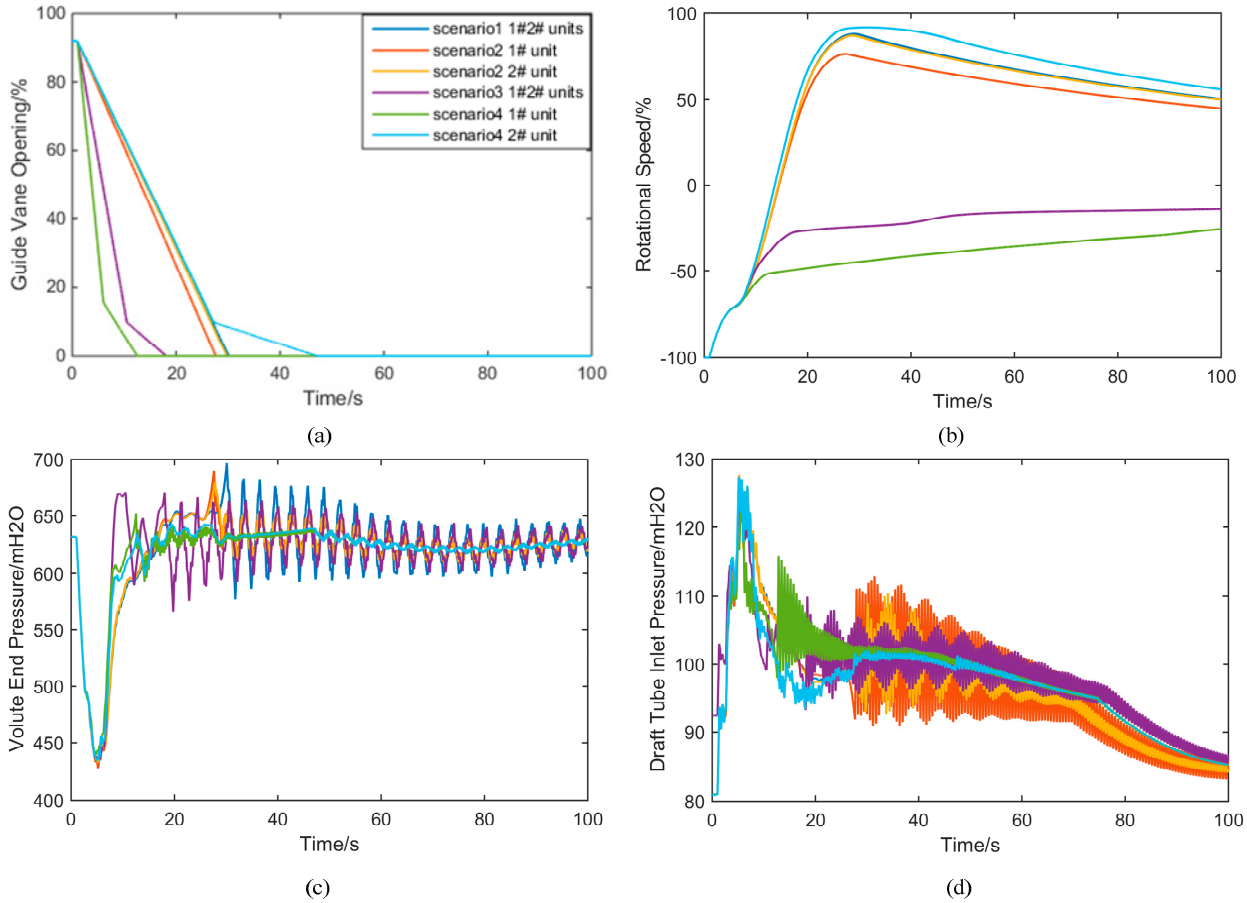

Fig.12 The transient process of 15 schemes by different scenarios

Table 7 The index values of 15 schemes by different scenarios (I)

scenario	volute end		Obj_x	draft inlet		volute end		Obj_x	draft inlet	
	min	max	%	min	max	min	max	%	min	max
	1#					2#				
scenario 1	427.9	696.7	87.89	84.51	114.9	427.9	696.7	87.89	84.51	114.9
scenario 2	427.7	690.3	76.73	83.14	124.8	432.7	679.9	87.04	84.09	127.6
scenario 3	436.2	670.8	-14	86	110.3	436.2	670.8	-14	86	110.3
scenario 4	439.6	652.4	-25.7	85.1	127.2	434.3	635.2	91.01	85.15	122.9

Table 8 The index values of 15 schemes by different scenarios (II)

scenario	upstream surge water level			downstream surge water level		
	initial	min	max	initial	min	max
scenario 1	734.52	700.5	726	182.64	175	192.5
scenario 2	734.52	700.7	725.8	182.64	175.1	192.3
scenario 3	734.52	704.9	722.6	182.64	177.1	191.6
scenario 4	734.52	703	724.2	182.64	176.1	192

6. Conclusion

In this paper, an EMOBCGSA method is proposed to solve the OGVCS problem while considering the various hydraulic and mechanical constraints. The significant innovations of the proposed method are mainly focused on the following three aspects: (1) Based on numerical calculation model of PSHU system, a multi objective optimization model is established, which includes hydraulic and mechanical multiple factors. (2) To improve the convergence speed and ergodicity of the algorithm, novel population reconstruction strategy, multi-objective adaptive chemotaxis operation and velocity update method, and EAS update and maintenance strategy is introduced to improve the standard BCGSA. (3) Heuristic constraint-handling strategy with eliminating and local search based on violation ranking is proposed to handle the various constraints of OGVCS problem instead of traditional penalty function, which can improve the computing efficiency. Finally, to verify the feasibility and effectiveness of the proposed EMOBCGSA method, the 'single tube-double units' type PSHU system model based on actual parameters of one PSP is established and Pareto non-inferior solutions under load rejection and pump outage condition by different scenarios are obtained. The comparison and analysis for optimization results between EMOBCGSA and others algorithms indicate that the proposed method can obtain better schemes with better Obj_{pre} and Obj_{x}, and the Pareto optimal solutions of EMOBCGSA possess the preferable quality and better distribution.

Acknowledgement

This work was supported by the National Natural Science Foundation of China (NSFC) (No. 51239004, 91547208 and 51579107).

References

1. Ge, Q., Solar and Wind Power in Hybird Energy Systems in China. *Savonia-ammattikorkeakoulu* **2014**.
2. Zhong, Y.; Lu, P.; Cao, C.; Jin, B.; Jiang, H., China's Advances in New Energy Technology and Advice on Future Development. *Sino-Global Energy* **2011**.
3. Anagnostopoulos, J. S.; Papantonis, D. E., Pumping station design for a pumped-storage wind-hydro power plant. *Energy Conversion & Management* **2007,** 48, (11), 3009-3017.
4. Ding, H.; Hu, Z.; Song, Y., Stochastic optimization of the daily operation of wind farm and pumped-hydro-storage plant. *Renewable Energy* **2012,** 48, (6), 571–578.
5. Petrakopoulou, F.; Robinson, A.; Loizidou, M., Simulation and analysis of a stand-alone solar-wind and pumped-storage hydropower plant. *Energy* **2016,** 96, (2), 676-683.

6. Kazempour, S. J.; Moghaddam, M. P.; Haghifam, M. R.; Yousefi, G. R., Risk-constrained dynamic self-scheduling of a pumped-storage plant in the energy and ancillary service markets. *Energy Conversion & Management* **2009,** 50, (50), 1368–1375.
7. De Marchis, M.; Milici, B.; Volpe, R.; Messineo, A., Energy Saving in Water Distribution Network through Pump as Turbine Generators: Economic and Environmental Analysis. *Energies* **2016,** 9, (11).
8. Pavesi, G.; Cavazzini, G.; Ardizzon, G., Numerical Analysis of the Transient Behaviour of a Variable Speed Pump-Turbine during a Pumping Power Reduction Scenario. *Energies* **2016,** 9, (7).
9. Wang, Z.; Zhu, B.; Wang, X.; Qin, D., Pressure Fluctuations in the S-Shaped Region of a Reversible Pump-Turbine. *Energies* **2017,** 10, (1).
10. Zeng, W.; Yang, J. D.; Hu, J. H.; Yang, J. B., Guide-Vane Closing Schemes for Pump-Turbines Based on Transient Characteristics in S-shaped Region. *Journal of Fluids Engineering-Transactions of the Asme* **2016,** 138, (5).
11. Azoury, P. H.; Baasiri, M.; Najm, H., Effect of Valve-Closure Schedule on Water Hammer. *Journal of Hydraulic Engineering* **1986,** 112, (10), 890-903.
12. Kuwabara, T.; Katayama, K.; Nakagawa, H.; Hagiwara, H. In *Improvements of transient performance of pump turbine upon load rejection*, Power Engineering Society Summer Meeting, 2000; 2000; pp 1783-1788 vol. 3.
13. Yu, X.; Zhang, J.; Miao, D., Innovative Closure Law for Pump-Turbines and Field Test Verification. *Journal of Hydraulic Engineering* **2015,** 141, (3), 05014010.
14. Zhang, J.; Hu, J.; Hu, M.; Fang, J.; Chen, N. In *Study on the Reversible Pump-Turbine Closing Law and Field Test*, ASME 2006 Joint U.s.-European Fluids Engineering Summer Meeting Collocated with the International Conference on Nuclear Engineering, 2006; 2006; pp 931-936.
15. Liu, J. T.; Liu, S. H.; Sun, Y. K.; Wu, Y. L.; Wang, L. Q., Numerical simulation of pressure fluctuation of a pump-turbine with MGV at no-load condition. *Iop Conference* **2012,** 15, (6), 2036.
16. Pannatier, Y.; Kawkabani, B.; Nicolet, C.; Simond, J. J.; Schwery, A.; Allenbach, P., Investigation of Control Strategies for Variable-Speed Pump-Turbine Units by Using a Simplified Model of the Converters. *IEEE Transactions on Industrial Electronics* **2010,** 53, (9), 3039-3049.
17. Sun, H.; Xiao, R.; Liu, W.; Wang, F., Analysis of S Characteristics and Pressure Pulsations in a Pump-Turbine With Misaligned Guide Vanes. *Journal of Fluids Engineering* **2013,** 135, (5), 511011.
18. Clarke, J.; Jr, M. L., Multi-objective particle swarm optimization of binary geothermal power plants. *Applied Energy* **2015,** 138, 302-314.
19. Wang, H. G.; Liang, M. A., Multi-objective particle swarm optimization. *Computer Engineering & Applications* **2008,** 45, (4), 82-85.
20. Deb, K.; Pratap, A.; Agarwal, S.; Meyarivan, T., A fast and elitist multiobjective genetic algorithm: NSGA-II. *IEEE Transactions on Evolutionary Computation* **2002,** 6, (2), 182-197.
21. Basu, M., Economic environmental dispatch using multi-objective differential evolution. *Applied Soft Computing Journal* **2011,** 11, (2), 2845-2853.
22. Lu, Y.; Zhou, J.; Hui, Q.; Ying, W.; Zhang, Y., Environmental/economic dispatch problem of power system by using an enhanced multi-objective differential evolution algorithm. *Energy Conversion & Management* **2011,** 52, (2), 1175-1183.
23. Li, C.; Zhou, J.; Peng, L.; Wang, C., Short-term economic environmental hydrothermal scheduling using improved multi-objective gravitational search algorithm. *Energy Conversion & Management* **2015,** 89, 127–136.
24. Ajami, A.; Armaghan, M., Application of multi-objective gravitational search algorithm (GSA) for power system stability enhancement by means of STATCOM. *International Review of Electrical Engineering* **2012,** 7, (4), 4954-4962.
25. Zhou, J.; Lu, P.; Li, Y.; Wang, C.; Yuan, L.; Mo, L., Short-term hydro-thermal-wind complementary scheduling considering uncertainty of wind power using an enhanced multi-objective bee colony optimization algorithm. *Energy Conversion & Management* **2016,** 123, 116-129.
26. Low; Hean, M. Y.; Chandramohan; Mahinthan; Choo; Seng, C., Application of multi-objective bee colony optimization algorithm to automated red teaming. **2009,** 2, (5), 1798-1808.

27. Xu, Y.; Zhou, J.; Xue, X.; Fu, W.; Zhu, W.; Li, C., An adaptively fast fuzzy fractional order PID control for pumped storage hydro unit using improved gravitational search algorithm. *Energy Conversion & Management* **2016,** 111, 67-78.
28. Wylie, Fluid Transients in Systems. *Prentice-Hall* **1993**.
29. Kung, C.; Yang, X., Energy interpretation of hydraulic transients in power plant with surge tank. *Journal of Hydraulic Research* **1993,** 31, (6), 825-840.
30. Vournas, C. D.; Papaioannou, G., Modelling and stability of a hydro plant with two surge tanks. *IEEE Transactions on Energy Conversion* **1995,** 10, (2), 368-375.
31. Zeng, Y.; Guo, Y.; Zhang, L.; Xu, T.; Dong, H., Nonlinear hydro turbine model having a surge tank. *Mathematical & Computer Modelling of Dynamical Systems* **2012,** 19, (1), 1-17.
32. Li, C.; Zhou, J., Parameters identification of hydraulic turbine governing system using improved gravitational search algorithm. *Energy Conversion & Management* **2011,** 52, (1), 374-381.
33. Xu, Y.; Zhou, J.; Zhang, Y.; Fu, W.; Zheng, Y.; Zhang, X. In *Parameter Optimization of Robust Non-fragile Fractional Order PID Controller for Pump Turbine Governing System*, 2016 Sixth International Conference on Instrumentation & Measurement, Computer, Communication and Control (IMCCC), 21-23 July 2016, 2016; 2016; pp 15-18.
34. Chen, Z.; Yuan, X.; Ji, B.; Wang, P.; Tian, H., Design of a fractional order PID controller for hydraulic turbine regulating system using chaotic non-dominated sorting genetic algorithm II. *Energy Conversion & Management* **2014,** 84, 390-404.
35. Eberhart, R. C.; Shi, Y. In *Particle swarm optimization: developments, applications and resources*, Evolutionary Computation, 2001. Proceedings of the 2001 Congress on, 2001; 2001; pp 81-86 vol. 1.
36. Chen, Z. H.; Yuan, X. H.; Tian, H.; Ji, B., Improved gravitational search algorithm for parameter identification of water turbine regulation system. *Energy Conversion and Management* **2014,** 78, 306-315.
37. Passino, K. M., Biomimicry of bacterial foraging for distributed optimization and control. *Control Systems IEEE* **2002,** 22, (3), 52-67.
38. Deb, K.; Mohan, M.; Mishra, S., Evaluating the ε-Domination Based Multi-Objective Evolutionary Algorithm for a Quick Computation of Pareto-Optimal Solutions. *Evolutionary Computation* **2005,** 13, (4), 501.
39. Kalyanmoy; Mohan; Manikanth; Mishra; Shikhar, *Towards a quick computation of well-spread pareto-optimal solutions*. Springer Berlin Heidelberg: 2003; p 222-236.